

# San Francisco gold deposit, Santa Ana region, Sonora, Mexico: Laramide orogenic, intrusion-related mineralization?

**K. Howard Poulsen**

*Consultant, Ottawa, Ontario, K2E 6B6, Canada*

**James K. Mortensen**

*Pacific Centre for Isotopic and Geochemical Research, University of British Columbia,  
Vancouver, British Columbia, V6T 1Z4, Canada*

**Phillip C. Walford**

*Marathon PGM Corporation, 330 Bay Street, Suite 1505, Toronto, Ontario, M5H 2S8, Canada*

## ABSTRACT

The million-ounce San Francisco gold deposit in the Llano district of northern Sonora State is composed of arrays of 1-10 cm thick, quartz-tourmaline-pyrite veins confined mainly to a stack of 1-10 m thick leucogranite sheets concordant with foliation in retrogressively metamorphosed felsic gneiss and amphibolite. The felsic gneiss in the mine area is unconformably overlain (at Cerro Gauna) by weakly metamorphosed Mesozoic metasedimentary and metavolcanic rocks possessing a steeply dipping cleavage, but also is in local tectonic contact with these units along the northward-dipping Llano Fault. Previous  $^{40}\text{Ar}/^{39}\text{Ar}$  dating studies of white mica from vein selvages at San Francisco indicates a minimum age of 41 Ma for mineralization in the leucogranite. Elsewhere in the Llano district, however, quartz veins containing gold and tourmaline are hosted by the Mesozoic metasedimentary rocks (at La Vetatierra) and cut granitoid rocks of the El Claro intrusion, suggesting a maximum age of 65 Ma for mineralization at that location. U-Pb zircon dating results at San Francisco demonstrate that the host leucogranite crystallized at approximately 1410 Ma (Mesoproterozoic) and overlying felsic to intermediate meta-ignimbrite above the unconformity at Cerro Gauna formed at approximately 180 Ma (Early Jurassic). Coupled with the previous data from San Francisco and a consideration of field relationships, this suggests a late Laramide timing of the deposits and a possible three-way link between gold and Laramide deformation and plutonism. Depending on perspective and scale, gold in the Llano district can be considered to be both “orogenic” and “intrusion-related”.

## INTRODUCTION

The Llano gold district in the Santa Ana region, Sonora, Mexico (Fig. 1), includes the San Francisco open-pit mine (Araiza-Martínez, 1998) and the smaller adjacent mine to the

west called La Chichara (Fig. 2). The combined heap-leach operation yielded 300,834 ounces gold production from 13.5 million tonnes mined between 1995 and 2001; current measured and indicated resources of 27.6 million tonnes are estimated to contain an additional 716,790 ounces gold (Timmins

e-mail: Poulsen: howardpoulsen@gmail.com; Mortensen: jmortensen@eos.ubc.ca; Walford: pwalford@sympatico.ca

Poulsen, K.H., Mortensen, J.K., and Walford, P.C., 2008, San Francisco gold deposit, Santa Ana region, Sonora, Mexico: Laramide orogenic, intrusion-related mineralization?, *in* Spencer, J.E., and Titley, S.R., eds., *Ores and orogenesis: Circum-Pacific tectonics, geologic evolution, and ore deposits*: Arizona Geological Society Digest 22, p. 547-559.

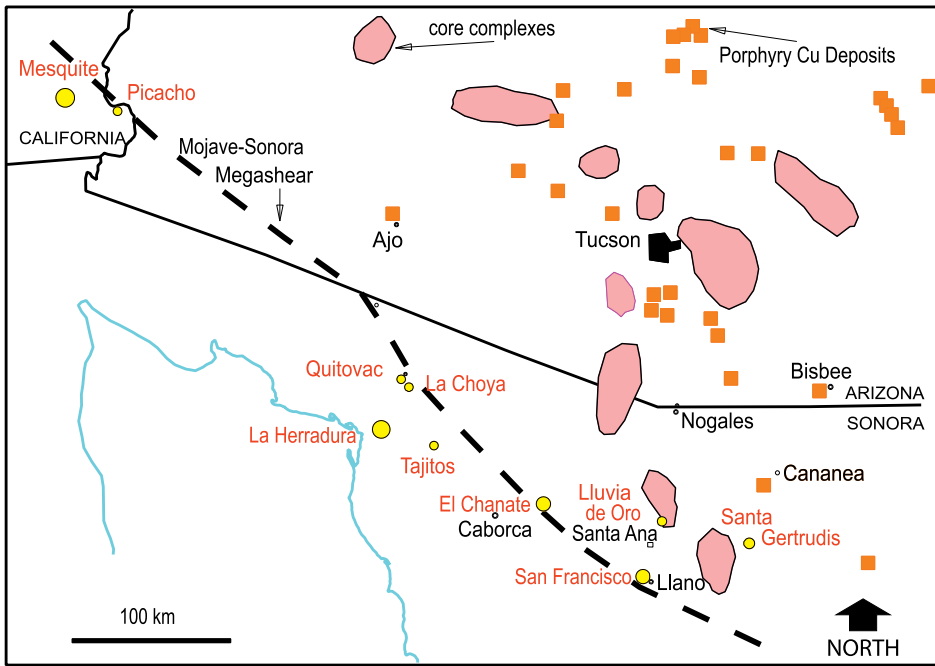
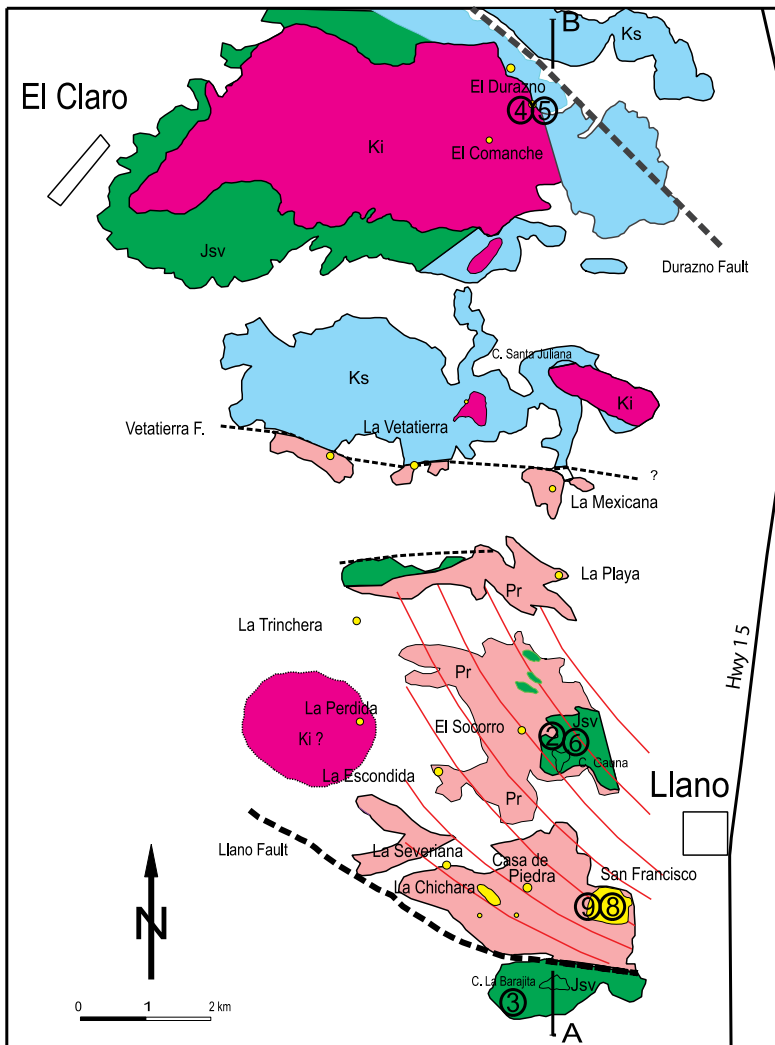


Figure 1. Simplified map of the Sonora-Mojave region showing selected structural features and porphyry copper and gold deposits. Metamorphic core complexes are stippled and the inferred position of the Mojave-Sonora megashear has been approximated from several published sources.



Gold Corporation, March 31, 2008). Placer gold was mined from the property by shafts through the overburden to the rock contact at least one hundred years ago. These old mines were destroyed by the open pit. Prior to open-pit mining, a minor amount of underground testing was conducted to confirm an area of abundant quartz veining that graded over 3 grams per tonne. The underground workings were also mined through by the pit. The majority of the gold mineralization is associated with quartz-vein sets in a leucogranite and, to a lesser extent, pegmatitic phases. The veins, up to 1 m thick, as well as the stringers and micro veins around them, contain dravite tourmaline and pyrite and have sericitic selvages. Pyrite cubes up to one centimeter on edge are common in the veins and surrounding altered rocks. Visible gold is rare in the veins and/or wall-rocks below the level of oxidation of 30 m. In the oxidation zone flakes of native gold were

Figure 2 (left). Geological map of the Llano gold district showing the location of gold deposits (dots). The circular outline near La Perdida marks a positive magnetic anomaly thought to be related to a buried intrusion. Location of samples for U-Pb zircon geochronology are labeled and circled. The line AB corresponds to the cross-section in Figure 3. Pr – San Francisco Gneiss and leucogranite; Jsv – Jurassic volcanic and clastic sedimentary rocks; Ks – Cretaceous limestone and clastic sedimentary rocks; Ki – Late Cretaceous intrusions. The red trend lines approximate the strike of foliation in the San Francisco gneissic units.

found near, on, and in oxidized pyrite cubes. Gold grades are highest in the deposit where the veins are in greatest abundance. Locally, grades can exceed 30 grams per tonne gold. High grade areas are commonly indicated by the presence of minor amounts of galena, sphalerite and rarely chalcopyrite. Much of the gold is sited in micro veins that form large alteration halos in wall-rock grading a gram or less. At Chichara, the gold veins and disseminations were in part hosted by amphibolite, likely metagabbro.

The Llano district is part of a broader gold belt extending northwestward to Mesquite, southeastern California (Fig. 1), approximating the trend of the contentious Mojave-Sonora megashear (Anderson and Silver, 1979, 2005; Molina-Garza and Iriondo, 2007) and the California-Coahuila transform (Dickinson and Lawton, 2001a). Gold deposits in this belt are of diverse type (Silberman et al., 1988; Jacques-Ayala and Clark, 1998) and more of them have been regarded to be “mesothermal” than “epithermal” (Pérez-Segura et al., 1996). Many different geological controls have been invoked for individual deposits in this gold belt, including reactivation of the Jurassic Mojave-Sonora megashear, Laramide deformation and intrusions, early Tertiary extension and detachment faults, Tertiary strike-slip faults, and emplacement of Early Tertiary “two-mica” granitoid rocks. Many of these geological elements are present in the Santa Ana region and have the potential to have played a role in forming the deposits in the Llano district (Fig. 2).

## GEOLOGY

The Llano gold district occupies a northerly trending series of ranges extending southward from the El Claro intru-

sion to the Llano Fault (Figs. 2 and 3).

The main geological observations pertinent to the localization of the gold deposits in the Llano district are as follows:

(1) Most of the known gold occurrences (Fig. 2) are located in an extensive body of Precambrian rock, the San Francisco gneiss. The gneiss was deformed under conditions of medium to high-grade metamorphism and deformation. It was derived in large part from Precambrian intrusive rocks including granitoid (likely tonalitic) and gabbroic (local amphibolite) compositions. Local lenses of marble attest to the fact that some gneiss may have formed from sedimentary or volcanic protoliths. Augen gneiss (Fig. 4A) is locally present and is likely derived from a pegmatitic granitic protolith. The variation in composition and texture of the gneiss impart a distinctive fabric to these Precambrian basement rocks. Apart from local variations, compositional layering and coplanar penetrative foliation strikes on average N30°W and dips moderately to steeply to the ENE (Fig. 2). The age and origin of the gneissic rocks has proven problematic. Salas (1968) regarded similar rocks north of Santa Ana in Cerro del Portera as Precambrian but other workers (e.g., Changkuon, 1990; Morales-Montaña, 1984) have interpreted them to be Jurassic in age. Pérez-Segura et al. (1996) used an  $^{40}\text{Ar}/^{39}\text{Ar}$  age of 911 Ma on hornblende to suggest the amphibolite was at least metamorphosed in the Neoproterozoic time, and hence represents a minimum age of the protolith. Calmus et al. (1992), however, suggested the Proterozoic rocks were also subjected to a Jurassic “Nevadan” deformation, an interpretation also favored by Anderson et al. (2005).

(2) The San Francisco gneiss is intruded by leucogranite that locally possesses a distinctive graphic and pegmatitic texture. The leucogranite does not appear to have been sub-

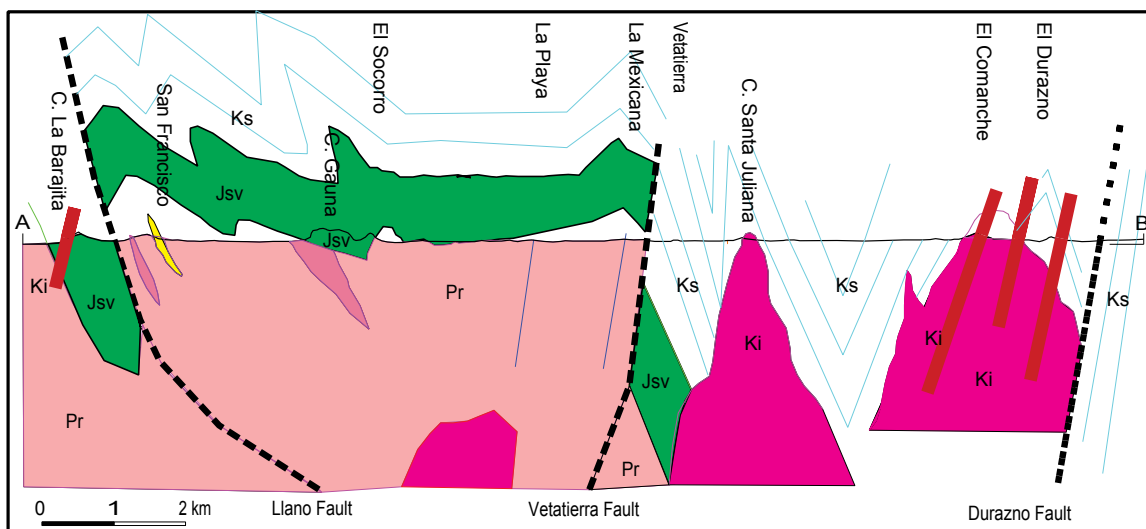


Figure 3. Schematic north-south cross-section from La Barajita through Cerro Gauna and Cerro Santa Juliana to Durazno. The section is accurate in horizontal scale but has been exaggerated vertically. Where uncertainties exist concerning the dips of faults they are shown to be vertical and the section has not been balanced. Note that most of the gold occurrences in this area occur in the wedge of gneiss bounded below by the Llano Fault and above by an angular unconformity. Legend as in Figure 2.

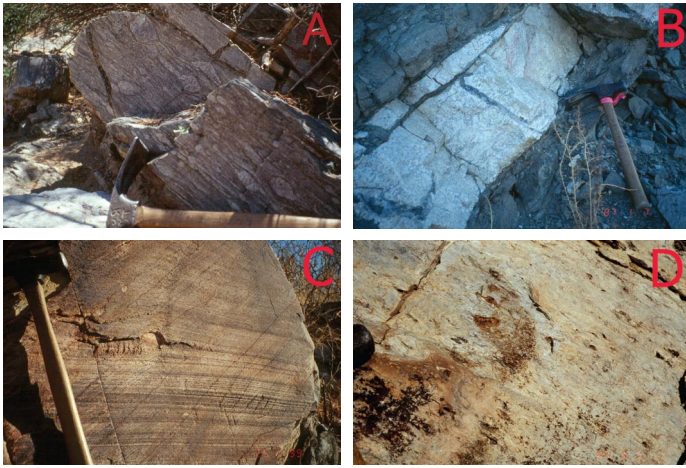


Figure 4. Key geological features in the Llano district: (A) Coarse orthogneiss; (B) leucogranite sheet (light) cutting gneiss but in turn cut by gold-quartz veins, San Francisco Mine; (C) bedded arenite cut obliquely by spaced metamorphic cleavage, Cerro Gauna; (D) foliated meta-rhyolite, Cerro Gauna; hammer head at left for scale.

jected to the same medium- to high-grade metamorphism as the gneiss and only locally displays a greenschist-facies foliation. Although the leucogranite is present in places as larger irregular masses, it occurs most commonly as 1- to 10-meter-thick sheets (Fig. 4B) concordant with gneissic layering in the country rocks. These “sills” of leucogranite are only locally weakly boudinaged in contrast to the high strain recorded in their host gneiss. Their concordance with the gneiss, however, indicates that a strong structural anisotropy was fully present in the host rocks at the time the leucogranite was emplaced. The leucogranite is a common host for gold-quartz veins (Fig. 4B) but its age was previously unknown, even though it has been assumed to be either Tertiary (Calmus et al., 1992; Pérez-Segura et al., 1996) or Jurassic (Changkuon, 1990).

(3) The San Francisco gneiss and leucogranite are unconformably and non-conformably overlain in depositional contact by conglomerate, sandstone and tuff belonging to the Coyotillo Group (Salas, 1968). In the area of the San Francisco mine, the unconformity closely mimics the modern-day erosional surface but to the south, folded rocks of the Coyotillo Group are juxtaposed against the gneiss along the Llano Fault (Figs. 2, 3). At Cerro Gauna, the rocks above the unconformity include metaconglomerate and metasandstone (Fig. 4C), locally containing detrital magnetite, as well as abundant meta-rhyolite units (Fig. 4D). Intercalation of the rhyolite and sandstone points to their coeval deposition. A key aspect of the sandstone and rhyolitic rocks is their greenschist-facies dynamothermal metamorphic foliation (Figs. 4C, D). Comparisons with regional descriptions suggest this stratigraphic package, which is up to one km in total thickness in this area, is part of the widespread Jurassic arc sequence and the overlying Glimpse Conglomerate of Arizona (e.g., Dickinson and Lawton, 2001b). Nonetheless some workers have assigned the section at Cerro

Gauna to the Tertiary and have portrayed the unconformity as a listric detachment fault (e.g., Anderson et al., 2005).

(4) In the northern half of the district, the Coyotillo Group is overlain by varicolored shale and siltstone as well as by distinctive fossiliferous limestone of the Represso (Bisbee equivalent) Group (Jacques-Ayala, 1992, 1995). The age of the shallow marine Mural limestone of the Represso Group is placed in the range 100-115 Ma on the basis of fossil assemblage (Jacques-Ayala, 1995). The rocks of the Represso Group have been folded and overprinted by a low-grade metamorphic foliation of similar orientation and style as observed in the Coyotillo Group. It is likely that the metamorphism corresponds to Late Cretaceous Laramide folding about NW-SE (fold) axes due to NE-SW shortening (Jacques-Ayala, 1992).

(5) The Llano Fault is the most significant dislocative structure in the San Francisco mine area. It is regarded as a thrust mainly because it places Precambrian San Francisco gneiss on Coyotillo Group rocks of presumed Jurassic age. There is, however, independent structural evidence that the Llano fault is a thrust. The first is that current mapping clearly shows that gneissic layering is deflected in the vicinity of the Llano fault (Fig. 2). Superficially, this might suggest a component of sinistral shear along the fault but this is misleading when one considers the geometry in three dimensions. The gneissic layering is discordant to the fault plane in both plan and section. Therefore reverse shear will result in the foliation being bent downward toward the fault about an axis parallel to the line of intersection of the fault and gneissic layering. The resulting deflection is therefore evident in both plan and section views. The corridor in the hanging wall of the Llano Fault where gneissosity is deflected from its predominant NNW strike corresponds to ductile deformation in the Llano Shear Zone. The effects at the outcrop scale are undoubtedly the observed low-grade shear zones nucleated along rheological contrasts and in pre-existing high-strain zones in the gneiss. It is also consistent with the fact that some competent units such as the leucogranite sheets, which post-date the deformation recorded by the gneiss, are locally boudinaged along their length. An additional line of evidence for the reverse movement on the Llano Fault is the fact that low-grade cleavage in folded Coyotillo Group rocks is consistently inclined to the north at moderate angle. Inasmuch as the perpendicular to cleavage is regarded to be an axis of finite shortening, in this case it corresponds to the direction consistent with contractional reverse movement on the Llano Fault (Fig. 3).

(6) A prominent geological feature of the Llano district is the El Claro granitoid intrusion (Fig. 2), which, along with smaller satellite bodies and local dikes, represents Laramide magmatism in the Llano district. Contact garnet-pyroxene skarn assemblages are developed along the margin of this body at El Durazno, where both the calc-silicate rocks are cut by a biotite-granite dike. Local granitoid dikes elsewhere in the district are likely of similar age. At Cerro La Barajita, one such dike cuts discordantly across folded and metamorphosed rocks of the Coyotillo Group. Near El Claro, the dynamother-

mal metamorphic cleavages in pelitic rocks in the aureole of the El Claro intrusion formed in the amphibolite facies; the resulting porphyroblastic biotite schist contains a prominent cleavage which in turn is crenulated. The overall impression is that the Laramide intrusions are late-kinematic with respect to dynamothermal metamorphism and deformation in the surrounding rocks.

(7) Gold mineralization in the Llano district occurs in several different structural sites (Fig. 5), the most common of which are fault-fill quartz veins. These planar veins, commonly 10- to 100-cm thick, occupy steep faults discordant to the gneissic layering. The most common strike of such veins is WNW, which is essentially parallel to the strike of the Llano Fault. The fault-fill veins were the sites of most historic small-scale bedrock mining from open cuts. Their gold content is likely erratic in distribution and, given that they are few and widely spaced, these veins are of little interest as bulk-mining targets except for the fact that they at least mark locations where gold is known to occur. The more attractive sites for large tonnage gold resources involve the formation of extensional veins (Fig. 4b). These are dominant in all productive zones identified thus far and occur mainly as arrays localized in leucogranite sheets. The veins are observed to dip moderately southward, perpendicular to the host leucogranite,

a reflection of stretching along the length of this body, or to be nearly subhorizontal and oblique to the host, suggesting shear along its margins. In some cases, vein spurs extend into adjacent incompetent rocks where they are deflected in a manner suggesting reverse shear after they formed. A third extensional site is thought to locally involve "kinking" of gneissic layering (Fig. 5). All of the sites for gold are therefore consistent with vein formation in rocks undergoing brittle-ductile deformation and kinematically consistent with reverse movement in the Llano Shear Zone. The main control on the location of gold, however, is not the Llano Fault directly, but subsidiary structures initiated on inherently weak zones in the gneiss. Gold quartz veins are also found locally in the Coyotillo Group and within the El Claro intrusion at El Durazno.

(8) The main post-ore feature in the district is a swarm of mafic to felsic dykes, which strike northwest and dip moderately northeast. Most of the dykes are composed of hornblende-phyric diorite but they are cut by a least one lamprophyre dyke dated at 27 Ma by the  $^{40}\text{Ar}/^{39}\text{Ar}$  method (Pérez-Segura et al., 1996). The dyke swarm is significant because, apart from brittle offsets along N-S basin-and-range faults, they record no deformation after their emplacement during a period of NE-SW extension. Their extensive distribution in the undeformed state precludes any significant effects in the San Francisco area of the mid-Tertiary ductile deformation which led to the formation of the Magdalena metamorphic core complex to the north (Nourse, 1995; Anderson et al., 2005). This further re-enforces the idea of the gold deposits in the Llano area having likely formed during Laramide contraction rather than Tertiary extension.

## GEOCHRONOLOGY

Apart from the data reported herein, the only chronological constraints on the ages of host rocks and veins are the  $^{40}\text{Ar}/^{39}\text{Ar}$  data of Pérez-Segura et al. (1996), the K-Ar data of Miranda-Gasca et al. (1998), and the paleontological data contained in Salas (1968) and Jacques-Ayala (1995).

Nine rock samples potentially suitable for U-Pb zircon dating were collected in 1999 from the Llano district (Fig. 2). Six of the samples yielded a significant amount of zircon, which was dated at the Pacific Centre for Isotopic and Geochemical Research (PCIGR) facility at the University of British Columbia, using both isotope dilution - thermal-ionization mass spectrometry (ID-TIMS) as described in Pigage and Mortensen (2004) and laser-ablation - inductively coupled plasma - mass spectrometry (LA-ICP-MS) modified somewhat from those described by Chang et al. (2006). Analytical data for the six samples are given in Tables 2 and 3 (Appendix) and shown graphically in Figures 6 and 7. Interpreted results are summarized in Table 1. The results demonstrate three distinct episodes of igneous activity in the district: Mesoproterozoic emplacement of leucogranite into the Mesoproterozoic San Francisco gneiss, Early Jurassic felsic volcanism above an unconformity on the leucogranite and gneiss, and Late Creta-

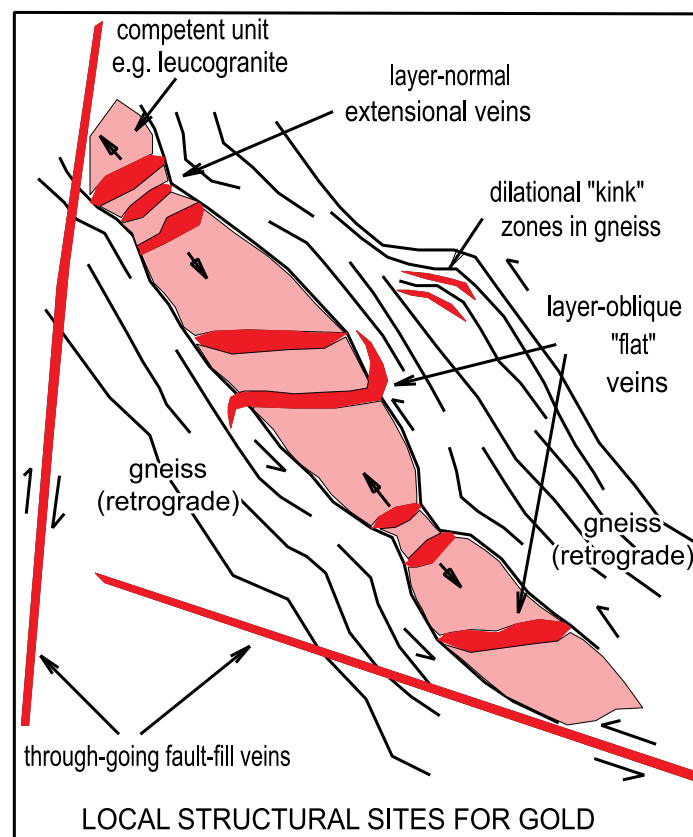


Figure 5. Schematic diagram showing relationships of quartz and quartz-tourmaline veins to structural features in the host rocks in both map and cross-sectional view.

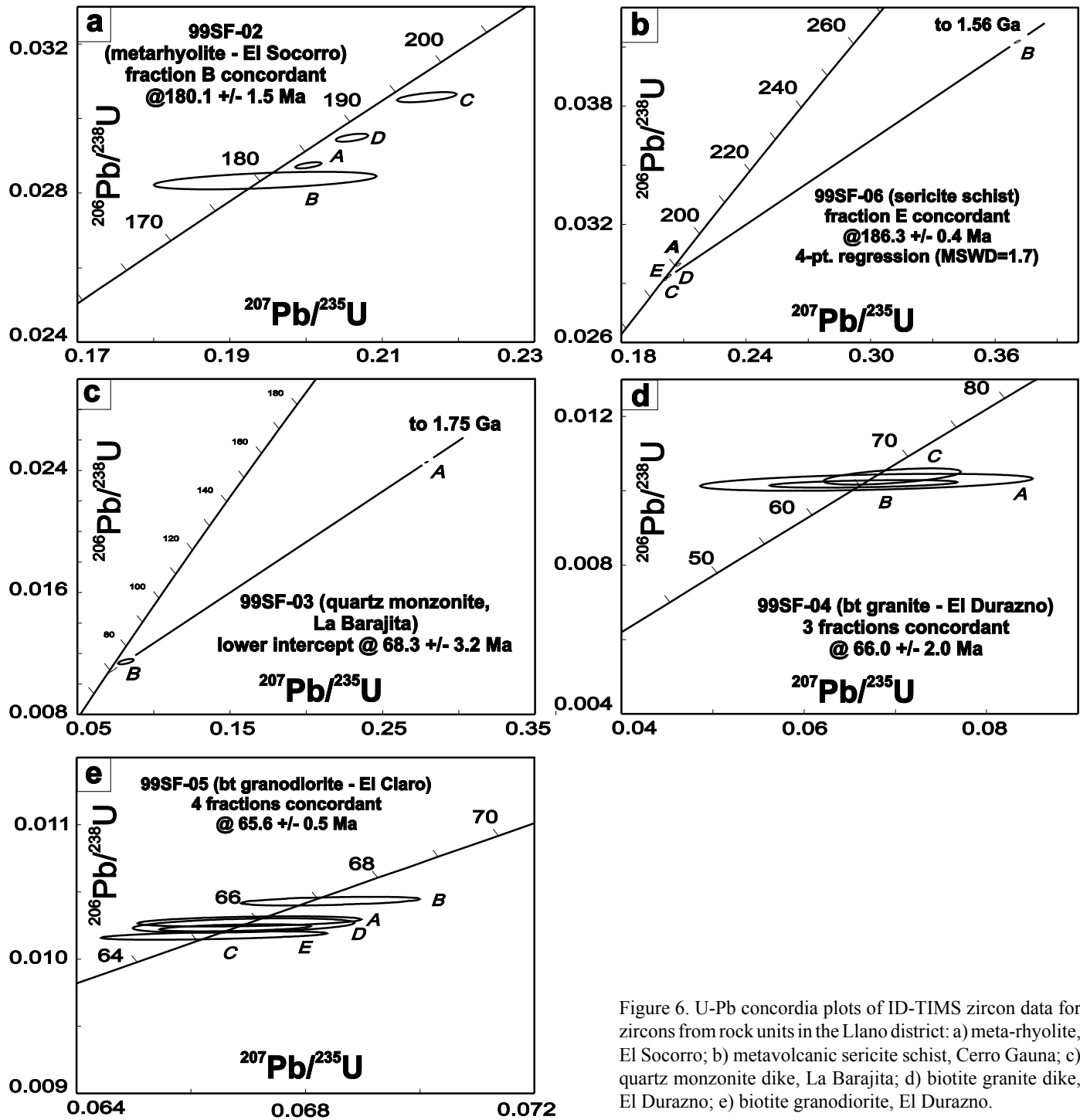


Figure 6. U-Pb concordia plots of ID-TIMS zircon data for zircons from rock units in the Llano district: a) meta-rhyolite, El Socorro; b) metavolcanic sericite schist, Cerro Gauna; c) quartz monzonite dike, La Barajita; d) biotite granite dike, El Durazno; e) biotite granodiorite, El Durazno.

Table 1: Results of U-Pb zircon geochronology of rocks from the Llano gold district.

Sample No.	UTM Coordinates (m), NAD 27	Rock Unit	Age (ID-TIMS)	Age (LA-ICP-MS)
99-SF-02	0487875E, 3360100N	Metarhyolite, El Socorro	180.1 ± 1.5 Ma	n/a
99-SF-06	0488300E, 3360400N	Sericite schist, Cerro Gauna	186.3 ± 0.4 Ma	n/a
99-SF-03	0487175E, 3356200N	Quartz monzonite, La Barajita	68.3 ± 3.2 Ma	n/a
99-SF-04	0487250E, 3370400N	Biotite granite, El Durazno	66.0 ± 2.0 Ma	n/a
99-SF-05	0487150E, 3370400N	Biotite granodiorite, El Durazno	65.5 ± 0.5 Ma	n/a
99-SF-08	0488700E, 3357325N	Leucogranite, San Francisco Mine	~1427 Ma	1404.2 ± 5.8 Ma
99-SF-09	0488350E, 3357575N	Gneiss (+ minor leucogranite), San Francisco Mine	1411.4 +3.2/ -2.9 Ma	1416.2 ± 7.4 Ma

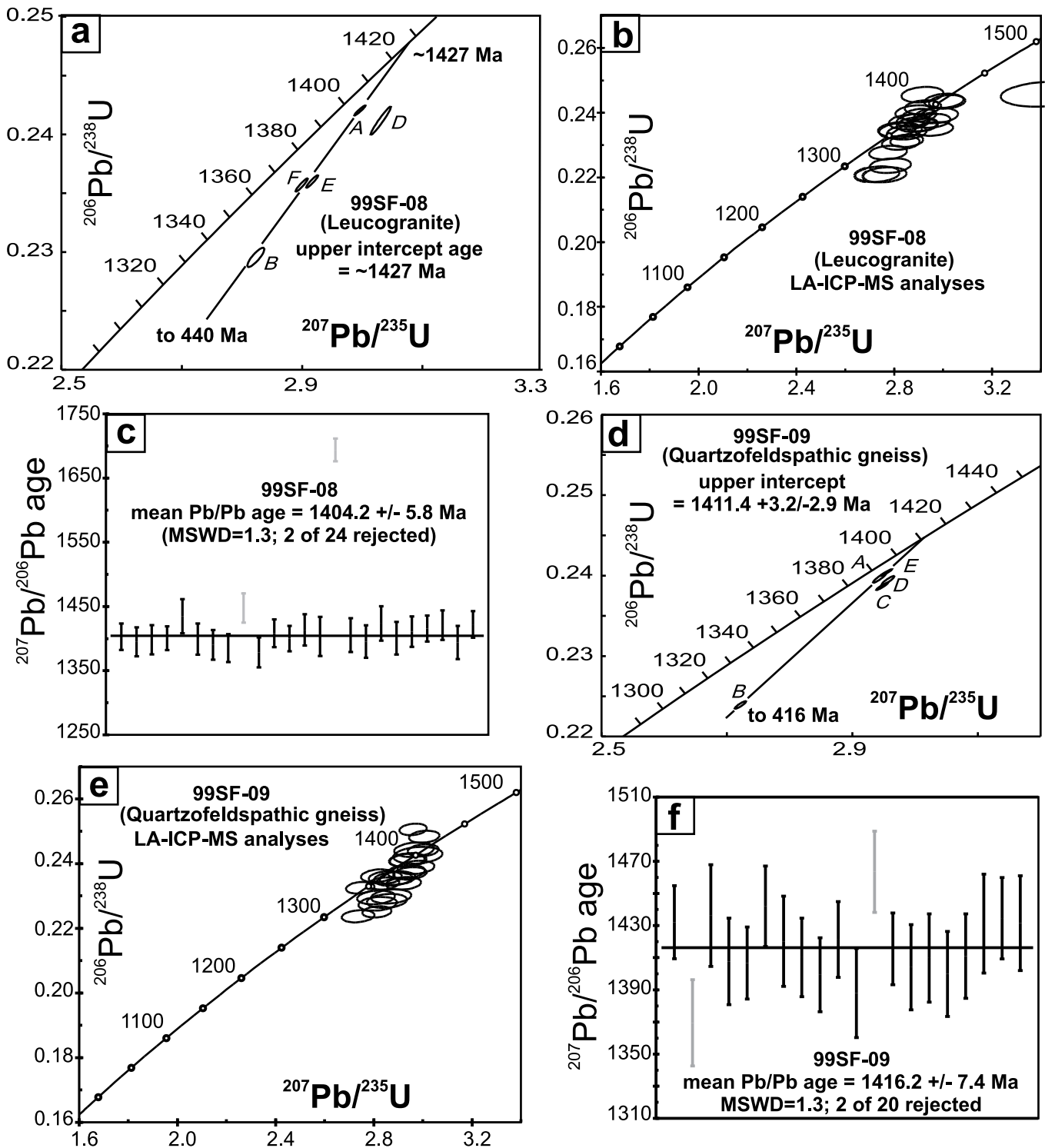


Figure 7. a) U-Pb concordia plots of ID-TIMS data for leucogranite sample 99-SF-08; b) corresponding LA-ICP-MS data for zircons from sample 8; c) Plot of Pb-Pb ages for sample 99-SF-8; d) Concordia plot for quartzofeldspathic gneiss sample 99-SF-09; e) corresponding LA-ICP-MS data for zircons from sample 9; f) Plot of Pb-Pb ages for sample 99-SF-09.

ceous intrusion of the El Claro granodiorite and related stocks and dykes. A fourth episode corresponds to emplacement of mafic dikes related to regional Mid-Tertiary volcanism (Pérez-Segura et al., 1996; Miranda-Gasca et al., 1998).

99-SF-02 is a sample of quartz-sericite schist (metahyalite) at El Socorro on the northwest side of Cerro Gauna.

It represents a felsic ignimbrite with metamorphic foliation suggesting probable equivalence with the Coyotillo Group but this unit has also been suggested to be Tertiary by some workers. Four fractions of abraded zircon were analyzed (Fig. 6a). Three are discordant, indicating the presence of minor inheritance of older zircon cores in some of the grains. One fraction

(B) gives a concordant analysis with a  $^{206}\text{Pb}/^{238}\text{U}$  age of  $180.1 \pm 1.5$  Ma, which we interpret as the crystallization age of the sample. It also provides a minimum age of underlying magnetite-bearing sandstone, which forms the base of the Coyotillo Group above an angular unconformity with basement gneiss and granitoid rocks of the San Francisco complex.

99-SF-06 is a sample of sericite schist from the northeast slope of Cerro Gauna. It is composed of welded vesicular and amygdaloidal metatuff. Five zircon fractions were analyzed (Fig. 6b). Three cluster on or very near concordia with fraction E giving a concordant analysis and a  $^{206}\text{Pb}/^{238}\text{U}$  age of  $186.3 \pm 0.4$  Ma, which we interpret as the crystallization age of the sample. Fraction A gives a slightly older age, indicating minor inheritance of older zircon. Fraction B yields a much older age, and a regression line through the cluster of nearly concordant analyses and this fraction gives a calculated upper intercept age of 1.56 Ga, which is an average age for the inherited zircon component in this fraction. The inherited component is presumably derived from underlying Precambrian rock units.

99-SF-03 is a sample of hornblende-plagioclase-phryic quartz monzonite from the southwest corner of Cerro La Barajita. The sample comes from a relatively undeformed dyke that cuts across folded Coyotillo Group metasedimentary rocks as well as the underlying San Francisco gneiss. The sample only yielded a very small amount of zircon, which was analyzed as two fractions. Both analyses are discordant (Fig. 6c), and a regression line through them gives calculated lower and upper intercept ages of  $68.3 \pm 3.2$  Ma and 1.75 Ga. We interpret the lower intercept age to give the approximate crystallization age for the body and the upper intercept as an average age for a substantial component of older inherited zircon in the sample. The crystallization age indicates that this is a Laramide dyke emplaced after much of the ductile deformation and metamorphism of the surrounding Mesozoic rocks. The  $\sim 1.75$  Ga inherited zircon component in this sample may be derived from either the underlying San Francisco gneiss or from detrital zircon components within the Coyotillo Group.

99-SF-04 is a sample of biotite granite from a dike in an open stope at El Durazno. The granite clearly cuts the larger mass of nearby biotite granodiorite and skarn developed in limestone at its contact. The biotite granite is cut by Au-quartz veins and by a porphyritic diorite dyke. Three fractions of abraded zircon give overlapping concordant analyses (Fig. 6d) with a total range of  $^{206}\text{Pb}/^{238}\text{U}$  ages of  $66.0 \pm 2.0$  Ma, which gives the crystallization age of the unit, and provides a confident maximum age of the Au quartz veins as well as minimum age of skarn.

99-SF-05 is a sample of biotite granodiorite representing the main mass of the El Claro intrusion directly west of El Durazno open stope. The biotite granodiorite cuts limestone and appears to postdate most ductile deformation in this area. At Durazno, the biotite granodiorite is cut by biotite granite dikes (sample 99-SF-04) and by quartz-tourmaline veins. Five zircon fractions were analyzed (Fig. 6e). Four of these give

overlapping concordant analyses (Fig. 6d) with a total range of  $^{206}\text{Pb}/^{238}\text{U}$  ages of  $65.5 \pm 0.5$  Ma, which we interpret as the crystallization age of the unit. One fraction (B) gives a concordant but slightly older age, which we interpret to indicate the presence of a minor inherited zircon component, perhaps from the early Jurassic metavolcanic rocks in the vicinity. This age is statistically identical to that obtained from the younger (from field relationships) biotite granite dyke, and therefore constrains the crystallization ages of both phases. The 65.5 Ma age also suggests that this is the minimum age of folds and cleavage as well as a maximum age of the contact skarn. Crenulation cleavages overprinting schist in the contact aureole of the intrusion on the southwest of the intrusion, however, suggest that some penetrative deformation took place after 65.5 Ma as well.

Samples of the leucogranite (99-SF-08) and quartzofeldspathic gneiss (99-SF-09) were initially analyzed using ID-TIMS methods on single grains (Figs. 7a and d). Analytical results showed some scatter, indicating the effects of both inheritance of older zircon components in some grains, and strong post-crystallization Pb-loss. In order to avoid these complications LA-ICP-MS methods were subsequently applied to zircons from each of these samples.

99-SF-08 is a sample of host leucogranite from the eastern side of 620 bench, San Francisco open pit. The granitoid rock is representative of the main host for the San Francisco orebody and is here cut by quartz-tourmaline veins and contains disseminated pyrite. The preferred age for this body is given by the weighted  $^{207}\text{Pb}/^{206}\text{Pb}$  age of  $1404.2 \pm 5.8$  Ma, which is based on a weighted average of the  $^{207}\text{Pb}/^{206}\text{Pb}$  ages of 21 of 24 grains that were analyzed (Fig. 7a and 7b). This age obviously represents a redundant maximum for mineralization, but more importantly provides a minimum age for the metagabbro and gneiss which are clearly cut by the leucogranite elsewhere in the pit.

99-SF-09 is a sample of quartzofeldspathic gneiss from the 668 bench in the central ore zone on the western side of the San Francisco open pit. The sample contains a narrow boudinaged granitoid dike which was sawed and separated from the rest of the sample prior to analysis. Initial ID-TIMS analyses on zircons separated from the gneiss suggested an age of 1411 Ma (Fig. 7d), although two of the five fractions analyzed gave slightly older ages, suggesting the presence of older inherited zircon components in at least some of the grains. The preferred U-Pb  $^{207}\text{Pb}/^{206}\text{Pb}$  zircon age of  $1416.2 \pm 7.4$  Ma is based on a weighted average of 18 of 20 analyses obtained using LA-ICP-MS methods (Fig. 7f). This age may correspond to the age of the protolith for this rock unit, if it is indeed meta-igneous in origin. The results from this sample are somewhat problematic, however, mainly because the sample has two identifiable components in hand sample, leucogranite and gneiss. The gneissic component clearly was deformed and metamorphosed prior to being cut by the leucogranite. It is possible therefore that the 1416 Ma age actually represents the age of the leucogranite component (which would have to

be a slightly older phase than that dated in sample 99-SF-08), rather than the age of the gneiss itself. An attempt was made during processing of the gneiss sample to avoid any of the leucogranite layers, however, and we therefore consider it probable that the age of 1416 Ma represents that crystallization age for the igneous protolith of the gneiss. Collectively the data for both samples leave no doubt about the Mesoproterozoic age of the leucogranite, although there remains some uncertainty about the age of the rest of the gneiss in the San Francisco complex, which may be reflected in the inherited 1750 Ma zircon component in sample 99-SF-03.

## DISCUSSION

The geological and geochronological data from the Llano district show that gold-quartz veins are constrained temporally to the interval between 65 and 40 Ma (Fig. 8), but spatially are related to faults and fractures in a variety of ages of hosts, in particular small bodies of Mesoproterozoic leucogranite. This observation is relevant to the local geological controls on the deposits, their relationship to the Laramide porphyry belt to the northeast, their relationship to the Mojave-Sonora megashear, their comparison with other deposits and districts in the Sonora-Mojave gold belt, and finally, their classification with respect to gold deposits in general.

The gold deposits of San Francisco and La Chichara comprise Laramide-age quartz veins in Precambrian leucogranite and gneiss. This refutes the earlier notion that the host leucogranite is Tertiary or Jurassic in age and that there is a genetic connection between the leucogranite and the veins cutting it (Calmus et al., 1992; Pérez-Segura et al., 1996; Jacques-Ayala

and Clark, 1996). It also rules out a direct connection with the mid-Tertiary detachment fault in the Magdalena core complex to the north (Changkuan, 1990). Furthermore, the fact that deformation recorded in the circa 180 Ma rocks of the Coyotillo Group affected Cretaceous strata as well largely rules out significant involvement of Jurassic deformation (Calmus et al., 1992; Anderson et al., 2005) in the history of this district. In spite of its value in eliminating some of these possibilities, the bracket on the age of mineralization, though much improved, is not particularly tight and this allows some leeway in interpreting the exact local controls on the deposits.

The fact that the gold-quartz veins at Durazno cut 65 Ma granitoid rocks raises the question as to whether there is an ultimate relationship between veining and the Laramide El Claro intrusion. Certainly this intrusion fits well into the range of ages for Cu-Mo deposits of the Laramide porphyry cluster to the northeast (Fig. 1). In fact, the geological setting of San Francisco, including the presence of leucocratic gneiss formed at circa 1400 Ma and an abundance of tourmaline in the hydrothermal products, is remarkably similar to that of the Cananea porphyry system. If the Llano gold deposits formed more or less contemporaneously with the porphyry deposits, the fundamental distinction would be one of differing crustal level. The evidence at San Francisco is for veins emplaced into an actively deforming environment at an unspecified but presumably moderate crustal depth.

The other permissible geological association for the Llano veins is with orogenic deformation. Regional considerations might suggest that this deformation is related to Jurassic deformation along the Mojave-Sonora megashear in some way (Anderson et al., 2005) but our data refutes this.

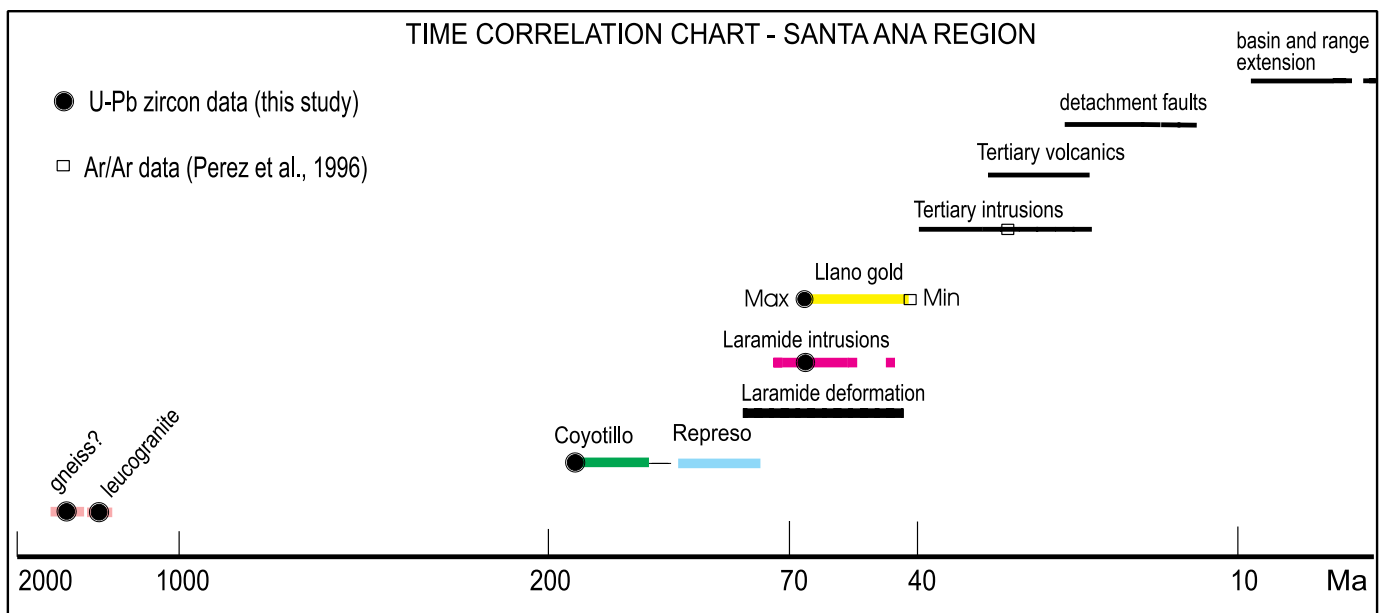


Figure 8. Time correlation chart showing the inferred age bracket of gold deposits in the Llano gold district in relation to regional geological events. The bracket is constrained by a maximum age for the El Claro intrusion and the minimum is based on the  $^{40}\text{Ar}/^{39}\text{Ar}$  studies of Pérez-Segura et al. (1996).

The field evidence suggests that most of the folding and shear zone development in the Llano district took place at greenschist facies conditions, postdated Cretaceous sedimentation, and pre-dated emplacement of the El Claro intrusion although some ductile deformation accompanied and post-dated it (i.e., cleavage in the contact aureole and ductile shear zones in the intrusion). Note, however, that the geological and geochronological evidence also indicates pre-Laramide, mid-Proterozoic deformation accompanied by amphibolite facies metamorphism to account for the augen gneiss and amphibolite. Furthermore, there is unequivocal evidence for gold-bearing quartz veins having been locally involved in syn- or post-vein ductile deformation as well and there is an inference that the veins at San Francisco actually formed during ductile boudinage of the host leucogranite. This Laramide deformation in the Llano district appears to be consistent with NE-SW shortening on the basis of cleavage and fold attitudes and on the interpretation of the Llano Fault as a steep thrust. The prevailing orientations of fault-fill and extensional veins, though not conclusive, can also be interpreted to be consistent with NE-SW compressive stress. Thus the bulk of the evidence at Llano points to a Laramide connection, either intrusive or structural or both. Unfortunately, the absolute age brackets on the veins are still relatively imprecise so that if they actually formed toward the younger side of the bracket (i.e., between 45 and 41 Ma) there may be other acceptable interpretations of local geological controls. These could include an unspecified early Tertiary transition from regional compression to extension (Calmus et al., 1992) or reactivation of an older structure such as the Mojave-Sonora megashear (Changkuon, 1990). Unlike Laramide deformation and magmatism, however, these geological events have not been independently established for this area.

The veins of the Llano district are part of a larger group of diverse Au deposits that occur throughout northern Sonora and into southern California. The veins at Llano have been specifically categorized as “structurally controlled” and share some similarities with “gneiss-hosted” or “metamorphic-hosted” deposits in southeastern California (Silberman et al., 1988). Our data accords well with the observations of Iriondo et al. (2005) at Quitovac (Fig. 1), where the structurally controlled gold-quartz vein deposits can also be shown to be directly associated with regional thrusting related to the Laramide orogeny between 65 and 48 Ma. East of the Llano district, at Santa Gertrudis and Amelia, and at El Chanate to the west, the gold deposits are sediment-hosted and in some cases, similar to those of Carlin-type (Silberman et al. 1988). The deposits at Tajitos are arguably epithermal vein deposits related to Jurassic arc rocks (Silberman et al., 1988) and at Mesquite, the deposit is thought to be composed of Tertiary epithermal veins (Willis and Tosdal, 1992). Thus, although Llano shares the distinction of being part of the Sonora-Mojave gold belt, it is unlikely that it shares a common age or origin with all of the other deposits defining the belt. The geologically most comparable deposits in terms of geological

setting in Precambrian metamorphic tectonites and the extensional vein style of mineralization appear to be La Herradura and Quitovac (Fig. 1).

Whether or not a Laramide age is accepted for the Llano district, there remains the issue of suitable global comparisons for the deposits found there. Perez et al. (1996) concluded the veins are “mesothermal” and correctly pointed out similarities of their characteristics compared to Archean analogues in the Abitibi gold belt in Canada. It has recently become fashionable to term such deposits as “orogenic” (Groves et al., 1998) rather than “mesothermal”; however, this has led to considerable confusion in their distinction from “intrusion-related” gold deposits (Sillitoe and Thompson, 1998). The veins at Llano arguably are “intrusion-related orogenic” gold deposits even though both aspects of this classification are of limited practical use. The deposits at San Francisco are intrusion-related in two different senses. First is the strong spatial correlation in the San Francisco area between veins and (Precambrian) leucogranite and second is the arguable temporal, and to a lesser degree spatial, association of the district as a whole with Laramide plutonism. The first correlation has been previously interpreted to be a genetic one (Calmus et al., 1992; Pérez-Segura et al., 1996); however, the Mesoproterozoic age of the leucogranite precludes this and indicates the cause is simply rheological. The second relationship is temporal but the precise genetic connection with Laramide magmatism is still unresolved. The deposits at Llano are also “orogenic” in the sense the veins intervene paragenetically between pre-mineral folding and cleavage development of regional extent in the cover rocks and continued post-mineral ductile deformation recorded in locally deformed veins. Thus to be more precise, the veins at Llano are “syn-orogenic”, a preferable designation since current usage of the orogenic classification commonly, and regrettably, includes “post-orogenic” deposits as well. Note also distinction of the Llano veins as both “intrusion-related” and “orogenic” provides no contradictions because, in tectonic terms, orogeny and magmatism commonly are not mutually exclusive. From a broader perspective, the Llano deposits share similarities with counterparts in the Tintina gold belt of Yukon and Eastern Alaska (Poulsen et al., 1997) and the Yanshanian gold belts of northern China (Poulsen and Mortensen, 1993). In all three cases there is a dominance of gold-quartz vein deposits controlled by regional stress fields in a continental crustal setting, in host rocks previously deformed in a ductile manner but approximately coincident with emplacement of Cretaceous intrusions of region extent. The Llano district is further analogous to the North China examples by the correlation with uplifts of Precambrian basement and by a strong influence of basement structure on the locations and orientations of younger veins.

## ACKNOWLEDGMENTS

The field observations were developed during collaboration with the Geomaque Geological Team operating in the

Llano area from 1999 through 2001. Hector Araiza, Daniel Maya, Luis Igrada, Salvador Siquiros, Andrés Castillo, Alejandro Acevedo and Mike Cooley made important contributions to the field work but the conclusions presented here are the sole responsibility of the authors. The manuscript has benefited from constructive reviews and comments by Alexander Iriondo, Efrén Pérez-Segura and the volume editors. The current owners of the project, Timmins Gold Corporation, are thanked for their permission to present the data in the public domain.

## REFERENCES

- Anderson, T.H., and Silver, L.T., 1979, The role of the Mojave-Sonora megashear in the tectonic evolution of northern Sonora, *in* Anderson, T.H. and Roldan-Quintana, J., eds., *Geology of northern Sonora: Geological Society of America Annual Meeting, Pittsburgh Pennsylvania, Guidebook, Trip 27*, p. 59–68.
- Anderson, T.H., and Silver, L.T., 2005, The Mojave-Sonora megashear – Field and analytical studies leading to the conception and evolution of the hypothesis, *in* Anderson, T.H., Nourse, J.A., McKee, J.W. and Steiner, M.B., eds., *The Mojave-Sonora megashear hypothesis: Development, assessment, and alternatives: Geological Society of America, Special Paper 393*, p. 1–50.
- Anderson, T.H., Rodríguez-Castañeda, J.L., and Silver, L.T., 2005, Jurassic rocks in Sonora, Mexico: Relations to the Mojave-Sonora megashear and its inferred northwestward extension, *in* Anderson, T.H., Nourse, J.A., McKee, J.W. and Steiner, M.B., eds., *The Mojave-Sonora megashear hypothesis: Development, assessment, and alternatives: Geological Society of America Special Paper 393*, p. 51–95.
- Araiza-Martínez, H., 1998, The San Francisco gold mine, Municipality of Santa Ana, Sonora, Mexico, *in* Clark, K.F., ed., *Gold Deposits of Northern Sonora, Mexico: Society of Economic Geologists, Guidebook Series, v. 30*, p. 49–58.
- Calmus, T., Pérez-Segura, E., and Herrera-Urbina, S., 1992, *Geology of Estación Llano (Sonora): A new Proterozoic basement and the San Francisco gold deposit*, *in* Clark, K.F., Roldan-Quintana, J. and Schmidt, R.H., eds., *Geology and mineral resources of northern Sierra Madre Occidental, Mexico; El Paso Geological Society, 1992 Field Conference Guidebook*, p. 313–321.
- Chang, S., Vervoort, J.D., McClelland, W.C., and Knaack, C., 2006, U-Pb dating of zircon by LA-ICP-MS: Geochemistry, Geophysics, Geosystems, v. 7, Q05009; doi:10.1029/2005GC001100.
- Changuon, L., 1990, *Genesis of gold mineralization, San Francisco Mine, Sonora, Mexico: unpublished MS thesis, New Mexico Institute of Mining and Technology, Socorro, New Mexico*, 129 p.
- Dickinson, W.R., and Lawton, T.F., 2001a, Carboniferous to Cretaceous assembly and fragmentation of Mexico: *Geological Society of America Bulletin*, v. 113, p. 1142–1160.
- Dickinson, W.R., and Lawton, T.F., 2001b, Tectonic setting and sandstone petrofacies of the Bisbee basin (USA-Mexico): *Journal of South American Earth Sciences*, v. 14, p. 475–504.
- Groves, D.I., Goldfarb, R.J., Gebre-Mariam, M., Hagemann, S.G., and Robert, F., 1998, Orogenic gold deposits: A proposed classification in the context of their crustal distribution and relationship to other gold deposit types: *Ore Geology Reviews*, v. 13, p. 7–27.
- Iriondo, A., Martínez-Torres, L.M., Kunk, M.J., Atkinson, W.W. Jr., Premo, W.R., and McIntosh, W.C., 2005, Northward Laramide thrusting in the Quitovac region, northwestern Sonora, Mexico: Implications for the juxtaposition of Paleoproterozoic basement blocks and the Mojave-Sonora megashear hypothesis, *in* Anderson, T.H., Nourse, J.A., McKee, J.W., and Steiner, M.B., eds., *The Mojave-Sonora megashear hypothesis: Development, assessment, and alternatives: Geological Society of America Special Paper 393*, p. 631–669.
- Jacques-Ayala, C., 1992, The Lower Cretaceous Bisbee Group near Santa Ana, Northern Sonora, Mexico, *in* Clark, K.F., Roldán-Quintana, J., and Schmidt, R.H., eds., *Geology and mineral resources of northern Sierra Madre Occidental, Mexico; El Paso Geological Society, 1992 Field Conference Guidebook*, p. 349–357.
- Jacques-Ayala, C., 1995, Paleogeography and provenance of the Lower Cretaceous Bisbee Group in the Caborca – Santa Ana area, northwestern Sonora, *in* Jacques-Ayala, C., Gonzalez-León, C.M., and Roldán-Quintana, J., eds., *Studies of the Mesozoic of Sonora and Adjacent Areas: Geological Society of America Special Paper 301*, p. 79–98.
- Jacques-Ayala, C. and Clark, K.F., 1998, Lithology, structure and gold deposits of northwestern Sonora, Mexico, *in* K.F. Clark, ed., *Gold Deposits of northern Sonora, Mexico: Society of Economic Geologists, Guidebook Series, v. 30*, p. 203–248.
- Miranda-Gasca, M.A., Gómez-Caballero, J.A., and Eastoe, C.J., 1998, Borate deposits of northern Sonora, Mexico: Stratigraphy, tectonics, stable isotopes and fluid inclusions: *Economic Geology*, v. 93, p. 510–523.
- Molina-Garza, R.S., and Iriondo, A., 2007, The Mojave-Sonora megashear: the hypothesis, the controversy, and the current state of knowledge, *in* Alaniz-Alvarez, S.A. and Nieto-Samaniego, A.F., eds., *Geology of México: Celebrating the Centenary of the Geological Society of México: Geological Society of America Special Paper 422*, p. 233–259.
- Morales-Montano, M., 1984, Bosquejo geológico del cuadrángulo Estación Llano-Imuris; *Boletín del Departamento de Geología, Universidad de Sonora, segunda época, v.1, n.1*, p. 25–49. (cited in Calmus et al., 1992).
- Nourse, J. A., 1995, Jurassic-Cretaceous paleogeography of the Magdalena region, northern Sonora, and its influence on the positioning of Tertiary metamorphic core complexes, *in* Jacques-Ayala, C., González-León, C.M. and Roldán-Quintana, J., eds., *Studies of the Mesozoic of Sonora and Adjacent Areas: Geological Society of America Special Paper 301*, p. 59–78.
- Pérez-Segura, E., Cheilletz, A., Herrera-Urbina, S., and Hanes, J.A., 1996, *Geología, mineralización, alteración hidrotermal y edad del yacimiento de oro de San Francisco, Sonora – un depósito mesotermal en el noroeste de México: Revista Mexicana de Ciencias Geológicas*, v. 13, p. 65–89.
- Pigage L.C., and Mortensen J.K., 2004, Superimposed Neoproterozoic and Early Tertiary alkaline magmatism in the La Biche River area, southeast Yukon Territory: *Bulletin of the Canadian Society of Petroleum Geology*, v. 52, p. 325–342.
- Poulsen, K.H., and Mortensen, J.K., 1993, Observations on the gold deposits of Eastern Hebei Province, China, *in* *Current Research, Part D: Geological Survey of Canada, Paper 1993-1D*, p. 183–190.
- Poulsen, K.H., Mortensen, J.K., and Murphy, D.C., 1997, Styles of intrusion-related gold mineralization in the Dawson-Mayo area, Yukon Territory, *in* *Current Research Part A, Geological Survey of Canada, Paper 1997-A*, p. 1–10.
- Salas, G., 1968, Areal geology and petrology of the igneous rocks of the Santa Ana region, northwest Sonora: *Boletín Soc. Geol. Mexicana*, v. 31, p. 11–63.
- Silberman, M.L., Giles, D.A., and Graubard, C., 1988, Characteristics of gold deposits in Northern Sonora, Mexico: A preliminary report: *Economic Geology*, v. 83, p. 1966–1974.
- Sillitoe, R.H., and Thompson, J.F.H., 1998, Intrusion-related vein gold deposits: types, tectono-magmatic settings and difficulties of distinction from orogenic gold deposits: *Resource Geology*, v. 48, p. 237–250.
- Willis, G.F., and Tosdal, R.M., 1992, Formation of gold veins and breccias during dextral strike-slip faulting in the Mesquite mining district, southeastern California: *Economic Geology*, v. 87, p. 2002–2022.

## APPENDIX

Table 2. Data from zircon analyses by isotope-dilution, thermal-ionization mass spectrometry (ID-TIMS).\*

Sample Description <sup>1</sup>	Wt (mg)	U (ppm)	Pb <sup>2</sup> (ppm)	<sup>206</sup> Pb/ <sup>204</sup> Pb <sup>3</sup> (meas.)	total common Pb (pg)	<sup>208</sup> Pb (%)	<sup>206</sup> Pb/ <sup>238</sup> U <sup>4</sup> (± % 1σ)	<sup>207</sup> Pb/ <sup>235</sup> U <sup>4</sup> (± % 1σ)	<sup>207</sup> Pb/ <sup>206</sup> Pb <sup>4</sup> (± % 1σ)	<sup>206</sup> Pb/ <sup>238</sup> U age (Ma; ± % 2σ)	<sup>207</sup> Pb/ <sup>206</sup> Pb age (Ma; ± % 2σ)
<b>Sample 99-SF-02 (metarhyolite, Cerro Gaona)</b>											
A: N5,+134	0.009	530	15.4	779	11	10.8	0.02875(0.15)	0.2003(0.43)	0.05054(0.36)	182.7(0.5)	219.9(16.8)
B: N5,+134	0.013	164	5.0	392	10	16.1	0.02834(0.42)	0.1946(3.75)	0.04982(3.56)	180.1(1.5)	186.7(162.0)
C: N5,+134	0.005	344	11.5	323	11	17.5	0.03057(0.22)	0.2158(0.90)	0.05120(0.80)	194.1(0.8)	250.0(36.8)
D: N5,+134	0.011	340	11.1	986	7	18.3	0.02949(0.18)	0.2060(0.52)	0.05068(0.45)	187.3(0.7)	226.2(20.6)
<b>Sample 99-SF-06 (metarhyolite)</b>											
A: N10,+134	0.054	262	8.6	1221	22	17.5	0.02996(0.14)	0.2074(0.28)	0.05021(0.19)	190.3(0.5)	204.9(8.9)
B: N10,+134	0.027	318	13.7	2509	9	12.1	0.04127(0.10)	0.3707(0.20)	0.06515(0.13)	260.7(0.5)	779.0(5.4)
C: N10,+134	0.036	305	9.8	2035	10	17.4	0.02920(0.12)	0.2011(0.24)	0.04994(0.16)	185.5(0.5)	192.2(7.3)
D: N10,+134	0.036	342	11.1	2868	8	18.0	0.02938(0.14)	0.2031(0.23)	0.05013(0.15)	186.7(0.5)	201.1(6.9)
E: N10,+134	0.027	316	10.2	2277	7	18.2	0.02931(0.10)	0.2013(0.42)	0.04981(0.38)	186.3(0.4)	186.4(17.5)
<b>Sample 99-SF-03 (quartz monzonite, La Barajita)</b>											
A: N10,-74,u	0.021	436	11.0	1515	9	9.5	0.02455(0.11)	0.2788(0.22)	0.08238(0.15)	156.3(0.3)	1254.6(5.9)
B: N10,-74,u	0.008	446	5.6	65	53	16.7	0.01146(0.76)	0.0818(3.14)	0.05173(2.71)	73.5(1.1)	273.3(123)
<b>Sample 99-SF-04 (biotite granite, El Durazno)</b>											
A: N2,+134	0.012	78	0.85	56	16	16.4	0.01023(1.11)	0.0668(13.6)	0.04739(13.17)	65.6(1.5)	68.8(640)
B: N2,+134	0.013	74	0.80	146	5	14.3	0.01019(0.50)	0.0665(7.72)	0.04736(7.5)	65.3(0.7)	67.2(385)
C: N2,+134	0.010	43	0.45	71	5	11.1	0.01038(1.05)	0.0696(5.4)	0.04863(4.88)	66.6(1.4)	130.2(229)
<b>Sample 99-SF-05 (biotite granodiorite, El Durazno)</b>											
A: N2,+149	0.060	182	1.9	608	12	12.2	0.01028(0.18)	0.0670(1.46)	0.04728(1.40)	65.9(0.2)	63.4(66.2)
B: N2,+149	0.092	202	2.1	906	13	10.7	0.01043(0.16)	0.0684(1.14)	0.04758(1.08)	66.9(0.2)	78.4(51.2)
C: N2,+149	0.085	198	2.0	586	18	11.1	0.01018(0.15)	0.0664(1.49)	0.04733(1.41)	65.3(0.2)	65.9(67.2)
D: N2,+149	0.080	233	2.4	707	17	11.6	0.01025(0.26)	0.0669(1.45)	0.04735(1.37)	65.7(0.3)	66.9(65.1)
E: N2,+149	0.080	182	1.9	669	14	11.5	0.01023(0.13)	0.0668(0.99)	0.04732(0.94)	65.6(0.2)	65.6(44.9)
<b>Sample 99-SF-08 (leucogranite, San Francisco Mine)</b>											
A: N2,134-149	0.046	652	160	73630	6	7.7	0.24204(0.09)	2.9960(0.16)	0.08977(0.08)	1397.3(2.2)	1420.7(2.9)
B: N2,134-149	0.056	800	186	4943	129	7.2	0.22955(0.18)	2.8231(0.25)	0.08920(0.14)	1332.2(4.3)	1408.3(5.3)
D: N2,134-149	0.043	5.2	1.2	67760	1	5.9	0.24117(0.25)	3.0308(0.28)	0.09115(0.08)	1392.8(6.2)	1449.6(2.8)
E: N2,134-149	0.066	859	199	89070	9	4.6	0.23600(0.11)	2.9166(0.17)	0.08963(0.08)	1365.9(2.8)	1417.7(2.9)
F: N2,134-149	0.058	816	193	101800	7	6.4	0.23570(0.12)	2.8993(0.18)	0.08921(0.08)	1364.3(2.9)	1408.7(2.9)
<b>Sample 99-SF-09 (gneiss + minor leucogranite), San Francisco Mine</b>											
A: N2,134-149	0.006	1345	309	26360	4	2.5	0.23974(0.13)	2.9435(0.18)	0.08905(0.08)	1385.3(3.2)	1405.2(3.0)
B: N2,134-149	0.009	1498	323	12130	15	2.9	0.22393(0.11)	2.7215(0.17)	0.08814(0.08)	1302.6(2.5)	1385.7(3.2)
C: N2,134-149	0.014	1009	230	49180	4	2.0	0.23868(0.10)	2.9474(0.16)	0.08956(0.08)	1379.8(2.4)	1416.2(2.9)
D: N2,134-149	0.020	741	171	16110	13	2.8	0.23940(0.12)	2.9566(0.17)	0.08957(0.08)	1383.6(2.9)	1416.4(3.1)
E: N2,134-149	0.017	805	187	43520	5	3.9	0.24039(0.09)	2.9539(0.15)	0.08912(0.08)	1388.7(2.1)	1406.8(2.9)

<sup>1</sup> N1, N2, N5 = non-magnetic at n degrees side slope on Frantz magnetic separator; grain size given in microns; u = abraded.

<sup>2</sup> radiogenic Pb; corrected for blank, initial common Pb, and spike

<sup>3</sup> corrected for spike and fractionation

<sup>4</sup> corrected for blank Pb and U, and common Pb

\* Isotopic analyses were performed at the Pacific Centre for Isotopic and Geochemical Research at the University of British Columbia.

**Table 3. Data from zircon analyses by laser-ablation, inductively coupled plasma mass spectrometry (LA-ICP-MS)\*.**

Analysis	Isotopic Compositions (1 sigma errors)					Isotopic Ages (1 sigma errors)					Background Corrected Counts per Second									
	<sup>207</sup> Pb/ <sup>206</sup> Pb	error	<sup>207</sup> Pb/ <sup>235</sup> U	error	<sup>207</sup> Pb/ <sup>206</sup> Pb	error	<sup>207</sup> Pb/ <sup>235</sup> U	error	<sup>206</sup> Pb/ <sup>238</sup> U	error	202	204	206	207	208	232	235	238		
99SF-08 1	0.09034	0.00056	2.85396	0.02833	0.23116	0.0008	1432.7	1369.9	7.46	1340.6	4.2	0	38	130185	11777	3822	23673	4068	545440	
99SF-08 2	0.0873	0.00065	2.77366	0.03409	0.22776	0.00092	1367.2	1348.5	9.17	1322.7	4.85	19	18	76162	6657	2513	16524	2367	323891	
99SF-08 3	0.09005	0.00079	2.74538	0.03978	0.22097	0.00103	1426.6	1340.8	10.78	1287	5.45	0	1	44380	4001	79	566	1437	194555	
99SF-08 4	0.08807	0.0007	2.85705	0.03761	0.23673	0.00101	1383.9	1370.7	9.9	1369.7	5.27	90	0	61007	5378	42	819	1857	249667	
99SF-08 5	0.089	0.00054	2.91187	0.02821	0.23669	0.0008	1404.2	1385	7.32	1369.5	4.19	74	0	158904	14153	10014	64545	4799	650621	
99SF-08 6	0.0908	0.00064	2.99236	0.0347	0.24156	0.00094	1442.3	1405.7	8.83	1394.8	4.86	76	2	124538	11315	1309	7435	3735	499685	
99SF-08 7	0.09391	0.00081	2.80589	0.03992	0.21897	0.00102	1506.3	1357.1	10.65	1276.4	5.38	11	36	55500	5214	1077	7520	1836	245688	
99SF-08 8	0.08936	0.0007	3.00547	0.03988	0.23912	0.00102	1411.7	1409	10.11	1382.1	5.32	0	0	69372	6201	3784	23469	2039	281247	
99SF-08 9	0.08884	0.0006	2.92544	0.03226	0.24352	0.00091	1400.6	1388.5	8.35	1405	4.71	0	0	117798	10466	3932	24746	3538	469095	
99SF-08 10	0.08841	0.00056	2.91539	0.02982	0.23944	0.00084	1391.3	1385.9	7.73	1383.8	4.39	0	0	146508	12864	4626	29264	4365	589379	
99SF-08 11	0.09029	0.00059	3.03309	0.03224	0.2432	0.00088	1431.7	1416	8.12	1403.3	4.57	34	0	124813	11269	2915	17386	3677	497804	
99SF-08 12	0.08791	0.00065	2.90421	0.03526	0.24529	0.00098	1380.6	1383	9.17	1414.1	5.09	0	0	114476	10062	5782	35813	3429	452732	
99SF-08 13	0.09048	0.00061	2.95523	0.03257	0.23589	0.00088	1435.7	1386.2	8.36	1365.3	4.6	42	5	141083	12759	4093	24742	4277	580391	
99SF-08 14	0.08956	0.00055	2.85539	0.02797	0.23733	0.00081	1416.1	1378.1	7.31	1372.8	4.22	87	0	202302	18107	5222	32915	6219	827275	
99SF-08 15	0.08864	0.00073	2.91688	0.0399	0.23701	0.00104	1396.3	1386.2	10.34	1371.2	5.44	9	0	83589	7403	4157	25097	2516	342313	
99SF-08 16	0.089	0.00064	2.8347	0.03359	0.23964	0.00093	1404.1	1377.6	8.78	1384.8	4.86	0	0	95367	8480	4418	26957	2916	386303	
99SF-08 17	0.08925	0.00066	2.89664	0.035	0.23596	0.00095	1409.5	1381	9.12	1365.6	4.93	0	20	89089	7942	4471	28186	2720	366629	
99SF-08 18	0.08858	0.00064	2.80564	0.03262	0.23456	0.00092	1395.1	1357	8.7	1358.4	4.78	20	6	110786	9801	727	4139	3467	458677	
99SF-08 19	0.08995	0.00066	2.86743	0.03417	0.23008	0.00092	1424.4	1372.1	8.98	1334.9	4.8	45	0	117155	10524	897	5493	3850	494562	
99SF-08 20	0.08944	0.00092	3.67082	0.06242	0.27165	0.00141	1556	1565	13.57	1549.2	7.13	42	0	41767	4021	8488	47858	1088	149349	
99SF-08 21	0.08992	0.00079	2.74221	0.03957	0.22152	0.00103	1424.1	1340	10.74	1289.9	5.46	0	0	55017	4939	1599	10725	1790	241327	
99SF-08 22	0.08936	0.00133	3.43909	0.0825	0.24437	0.00175	1612.1	24.69	18.87	1409.4	9.06	0	0	18001	1785	2447	16250	516	71585	
99SF-08 23	0.09037	0.00063	2.94908	0.03295	0.23681	0.0009	1433.4	1319	13.94	1394.6	8.47	7	0	143255	12921	5078	31866	4357	587940	
99SF-08 24	0.08984	0.00073	2.8141	0.03701	0.23423	0.00101	1422	1359.3	9.85	1356.6	5.28	0	0	78756	7060	3648	24134	2496	326819	
99SF-09 1	0.0884	0.0005	2.72922	0.02509	0.23347	0.00077	1391.2	10.88	1336.4	6.83	1352.7	4.01	0	125116	11115	16713	107931	3977	516958	
99SF-09 2	0.08842	0.00055	2.87205	0.02963	0.23872	0.00084	1391.7	11.89	1374.6	7.77	1380	4.39	0	98235	8729	12713	81455	2968	397014	
99SF-09 3	0.08853	0.00055	2.93319	0.03041	0.24214	0.00086	1394	11.88	1390.5	7.85	1397.8	4.44	29	0	97407	8665	12125	73306	2886	388145
99SF-09 4	0.09033	0.00066	2.8636	0.03525	0.22891	0.00093	1432.3	1372.4	9.26	1328.8	4.86	84	3	60094	5452	5628	34790	1862	253417	
99SF-09 5	0.08987	0.00062	2.96676	0.03425	0.23813	0.00091	1422.7	1391.1	8.77	1377	4.75	67	0	74032	6681	9796	63283	2203	300131	
99SF-09 6	0.0886	0.00057	2.7958	0.02934	0.23375	0.00084	1395.5	1354.4	7.85	1354.1	4.39	0	40	107851	9552	14572	89892	3160	439253	
99SF-09 7	0.0882	0.00052	2.96859	0.02882	0.23709	0.0008	1386.9	11.28	1397.1	7.39	1371.6	4.17	0	107851	9552	14572	89892	3160	439253	
99SF-09 8	0.09115	0.00059	2.88953	0.03072	0.23451	0.00085	1449.6	12.2	1379.2	8.02	1358.1	4.45	0	80664	8203	18	218	2781	369320	
99SF-09 9	0.08664	0.00057	2.71945	0.02901	0.22582	0.00082	1352.5	12.54	1333.8	7.92	1312.6	4.31	0	90678	7885	28	262	2841	387909	
99SF-09 10	0.08922	0.00052	2.83318	0.02708	0.23361	0.00079	1408.9	11.18	1364.4	7.17	1353.4	4.11	0	122890	11004	15184	81898	3806	508253	
99SF-09 11	0.08892	0.00048	3.01713	0.02635	0.2462	0.00077	1402.4	1412	6.66	1418.8	4	0	0	171223	15278	22839	128950	4964	672000	
99SF-09 12	0.08978	0.00061	2.93996	0.03322	0.24175	0.00091	1420.8	12.88	1392.3	8.56	1395.8	4.75	0	82626	7442	286	1875	2483	330362	
99SF-09 13	0.08831	0.00074	2.98988	0.04318	0.24182	0.0011	1389.2	16.01	1405	10.99	1396.1	5.7	0	11	44892	3976	256	1350	179460	
99SF-09 14	0.08859	0.00062	2.80963	0.03271	0.22861	0.00089	1395.3	13.39	1358.1	8.72	1327.2	4.66	0	1	73995	6574	10565	65766	2297	312949
99SF-09 15	0.08835	0.0006	2.96433	0.03379	0.24485	0.00093	1390.2	13	1398.5	8.66	1411.8	4.81	87	0	82351	7294	11242	68281	2418	325308
99SF-09 16	0.08965	0.00064	2.87441	0.03411	0.23012	0.00091	1418.1	13.57	1375.2	8.94	1335.1	4.74	0	6	70889	6371	9148	57023	2178	297992
99SF-09 17	0.08869	0.0006	2.87999	0.03221	0.23588	0.00089	1397.3	12.89	1376.7	8.43	1365.3	4.62	1	18	82156	7303	9852	62021	2943	336942
99SF-09 18	0.0893	0.00059	2.98461	0.03301	0.23847	0.00088	1410.6	12.56	1403.7	8.41	1378.7	4.59	0	24	100841	9025	12982	80143	2974	409134
99SF-09 19	0.08931	0.0005	3.0344	0.0278	0.24496	0.0008	1410.7	10.75	1416.3	7	1412.4	4.12	51	0	156292	13985	17989	108044	4536	617521
99SF-09 20	0.08922	0.00057	2.91452	0.03041	0.23399	0.00084	1408.9	12.1	1385.7	7.89	1355.4	4.36	37	0	115151	10293	43	291	3477	476350
99SF-09 21	0.08895	0.00063	2.82246	0.03273	0.22761	0.00088	1403.1	13.4	1361.5	8.69	1322	4.63	55	0	79785	7109	40	373	2480	339338
99SF-09 22	0.08935	0.00052	2.78935	0.02605	0.22453	0.00075	1411.7	11.12	1352.7	6.98	1305.8	3.93	44	0	11851	13590	7176	44760	4800	654772

\* Isotopic analyses were performed at the Pacific Centre for Isotopic and Geochemical Research at the University of British Columbia.

